

## Article

# Effect of Extrusion Ratio on the Microstructure and Mechanical Properties of Al-0.5Mg-0.4Si-0.1Cu Alloy

Changan Ni <sup>1</sup>, Xingchuan Xia <sup>1,\*</sup> , Jiahang Dai <sup>1</sup>, Jian Ding <sup>1,\*</sup>, Yao Wang <sup>1</sup>, Jiangbo Wang <sup>1</sup> and Yongchang Liu <sup>2</sup><sup>1</sup> School of Material Science and Engineering, Hebei University of Technology, Tianjin 300130, China<sup>2</sup> School of Material Science and Engineering, Tianjin University, Tianjin 300130, China

\* Correspondence: xc\_xia@hebut.edu.cn (X.X.); djian0122@126.com (J.D.);

Tel./Fax: +86-22-60202011 (X.X. &amp; J.D.)

**Abstract:** Al-0.5Mg-0.4Si-0.1Cu alloy possessing weather resistance and oxidation resistance can obtain good surface quality (metallic luster) without chrome plating. Therefore, it is an important material to replace polluting chrome-plated aluminum profiles for automotive decorative parts. At present, studies about the extrusion process of Al-0.5Mg-0.4Si-0.1Cu alloy are very few, which affects its further application. In this work, the effect of extrusion ratios on microstructure and mechanical properties of Al-0.5Mg-0.4Si-0.1Cu alloy is investigated by optical microscopy (OM), scanning electron microscopy (SEM), electron backscattered diffraction (EBSD), transmission electron microscopy (TEM) and tensile tests. The results showed that the dynamic recrystallization degree of the alloy gradually increased with the extrusion ratio increasing, which is attributed to the driving force provided by the large extrusion ratio. Meanwhile, due to the occurrence of dynamic recrystallization, the texture changed from  $\langle 111 \rangle$  to  $\langle 001 \rangle$  orientation. In addition, grains were obviously refined and uniform with the extrusion ratio increasing. Due to the fine grain strengthening mechanism, the tensile strength and elongation of the alloy with an extrusion ratio of 30 reached 152 MPa and 32.4%.

**Keywords:** Al-0.5Mg-0.4Si-0.1Cu alloy; extrusion ratio; dynamic recrystallization; mechanical properties



**Citation:** Ni, C.; Xia, X.; Dai, J.; Ding, J.; Wang, Y.; Wang, J.; Liu, Y. Effect of Extrusion Ratio on the Microstructure and Mechanical Properties of Al-0.5Mg-0.4Si-0.1Cu Alloy. *Metals* **2023**, *13*, 669. <https://doi.org/10.3390/met13040669>

Received: 20 February 2023

Revised: 24 March 2023

Accepted: 25 March 2023

Published: 28 March 2023



**Copyright:** © 2023 by the authors. Licensee MDPI, Basel, Switzerland. This article is an open access article distributed under the terms and conditions of the Creative Commons Attribution (CC BY) license (<https://creativecommons.org/licenses/by/4.0/>).

## 1. Introduction

Due to their high toughness, lightweight and excellent corrosion resistance, Al–Mg–Si (–Cu) alloys have been widely used in automotive, construction and aerospace fields [1–4]. In recent years, Al–Mg–Si(–Cu) alloys have been investigated intensively. It is generally accepted that reasonable control of alloy composition can improve its microstructure and overall performance. It has been found that Mg and Si have a significant effect on the properties of Al–Mg–Si(–Cu) alloys. The strength of alloy with a low Mg/Si ratio was increased due to the promotion of aging precipitation. Meanwhile, modulating Mg/Si ratio can also improve its corrosion resistance [5–7].

In addition, it was demonstrated that the trace elements could significantly refine grains and reduce segregation which can improve the microstructure of the Al–Mg–Si(–Cu) alloys [8–11]. Prior studies also showed that the hot extrusion process has a significant effect on the microstructure of the alloy. During hot deformation, coarse equiaxed grains gradually evolved into fine equiaxed grains due to dynamic recrystallization [12]. In the study of the extrusion process of Al–Mg–Si(–Cu) alloys, Cao et al. [13] found that with the increase of the extrusion ratio, the dynamic recrystallization was more sufficient and the microstructure was more uniform. Moreover, the mechanical properties of the alloy were highest at large extrusion ratios. Zhang et al. [14] analyzed the microstructure evolution during the extrusion process, the results showed that with the increase of plastic deformation, more fine equiaxed grains were formed and the frequency of low-angle grain boundaries gradually decreased, which reflected the increase of recrystallization

degree. Therefore, the comprehensive properties of Al–Mg–Si(–Cu) alloy can be enhanced by reasonable composition regulation and extrusion processes.

Based on this, Al-0.5Mg-0.4Si-0.1Cu alloy possesses excellent weather resistance and oxidation resistance was developed, which can maintain a long period of metallic luster. Therefore, this alloy is expected to replace the polluting chrome-plated aluminum profiles for automotive decorative parts (such as luggage racks and window trim). Most decorative parts with complex structures were obtained by extrusion, and their microstructure and properties were easily affected by the hot extrusion process. Consequently, a comprehensive understanding of the influence of extrusion process parameters on the microstructure and mechanical properties of the alloy is important to facilitate its application. While, up to date, most of the research on Al-0.5Mg-0.4Si-0.1Cu alloy is focused on metallurgical processes, few studies reported the extrusion process of this alloy, especially about the effect of extrusion ratios ( $\lambda$ ) on its microstructure and mechanical properties. Therefore, in this work, the effect of extrusion ratios on the microstructure and mechanical properties of the alloy was studied through optical microscopy, scanning electron microscopy, electron backscattered diffraction, transmission electron microscopy and tensile tests. Moreover, the evolution mechanism of microstructure was explored which provides a theoretical basis for its production.

## 2. Materials and Experiment Procedures

### 2.1. Specimens Preparation

The raw material used in this work is commercial Al-0.5Mg-0.4Si-0.1Cu alloy (hereinafter referred to as the alloy) with its chemical composition shown in Table 1. The sample with the dimensions of  $\Phi 55 \times 100$  mm was selected at the positions possessing similar solidification parameters to ensure composition accuracy. The cylindrical billets were homogenized at  $540 \pm 1$  °C for 13 h in SX-G0413 high-temperature electric furnace (Zhonghuan Electric Furnace Inc., Tianjin, China), and then air-cooled. Based on the previous research results [15], 480 °C is considered the reasonable extrusion temperature. Extrusion tests were performed on a TXCJ-300 extruder (Yuchun Machinery Inc., Wuxi, China) with extrusion ratios of 7, 13, 21 and 30, respectively. In order to prevent the deformation heat of the billet and friction heat caused by the extrusion process temperature deviation, the preheating temperature of the die and extrusion barrel should be set lower than the billet temperature of about 20 °C. The hot extrusion process is as follows: First, the extruded billets were placed into the high-temperature electric furnace for heating and holding. Then, the heating coil of the extrusion cylinder was adjusted to a predetermined temperature. Finally, start the extruder and install the die when the extruded billets were heated for 1 h, followed by the billet into the extrusion barrel for hot extrusion. Due to the effect of a temperature drop on the accuracy of the experimental results, it is required to transfer the billet quickly.

**Table 1.** Chemical composition of Al-0.5Mg-0.4Si-0.1Cu alloy (wt.%).

Mg	Si	Cu	Fe	Mn	Zn	Ti	Cr	Al
0.466	0.394	0.114	0.023	$\leq 0.0030$	$\leq 0.0037$	$\leq 0.0052$	$\leq 0.0005$	Bal

### 2.2. Microstructure Observation

Figure 1 shows the positions of the samples used for microstructure observation and mechanical property testing. Typical metallographic preparation methods were used for metallographic specimens, that is, specimens were polished after grinding by different sandpapers (600#, 800#, 1000#, 1200#, 1500#, 2000#, 2500#). The metallographic specimens were etched with 2 vol.% HF solution for 4 min and then rinsed with ethanol. Leica DM2700M metallographic microscope (Leica Inc., Weztlar, Germany) was used for microstructure observation. Gemini SEM 300 (Zeiss Inc., Oberkochen, Germany) was used for electron backscatter diffraction and the observation position is the longitudinal section

of the alloy along the extrusion direction. The FEI Tecnai G2 F30 (FEI Inc., Hillsboro, OR, USA) was used for TEM observation, operating at 200 kV. The preparation process of the specimens for TEM observation was as follows: The samples were firstly thinned to 50–60  $\mu\text{m}$ , followed by punching into  $\Phi 3$  mm discs using a sample puncher. After that double-jet thinner (MTP-1A) and Ion thinning (Gatan 691) were used to obtain the thin zone. Liquid nitrogen was used for cooling during the experiment.

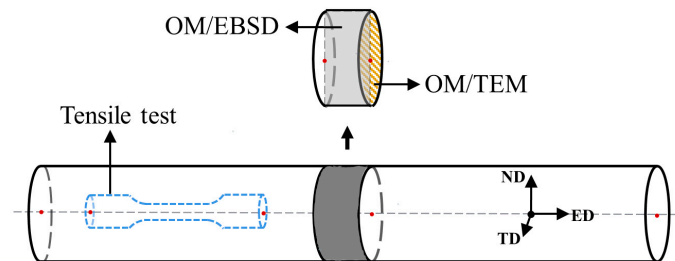


**Figure 1.** Schematic location of microstructure observation and tensile specimens.

### 2.3. Tensile Test

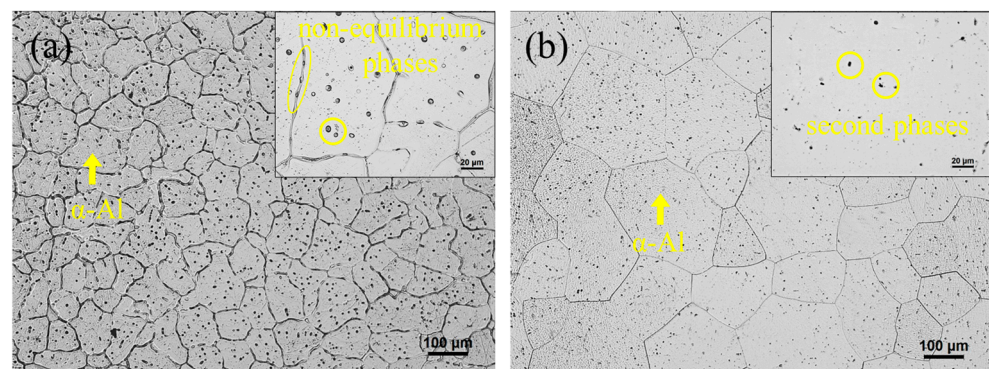
In order to establish the relationship between mechanical properties and the extrusion process, tensile tests were applied to the alloys with different extrusion ratios in this study.

Tensile test samples of extruded alloys were prepared according to the national standard of GB/T228-2010, and the sampling direction was the extrusion direction. The tensile test was obtained by UTM5105X universal test machine (Liantai Inc., Jinan, China) with a stretching speed of 2 mm/min. Three specimens of the same condition were selected for testing and the average values of tensile strength, yield strength and elongation of the alloys were obtained, respectively.

## 3. Results and Discussion

### 3.1. Homogenization

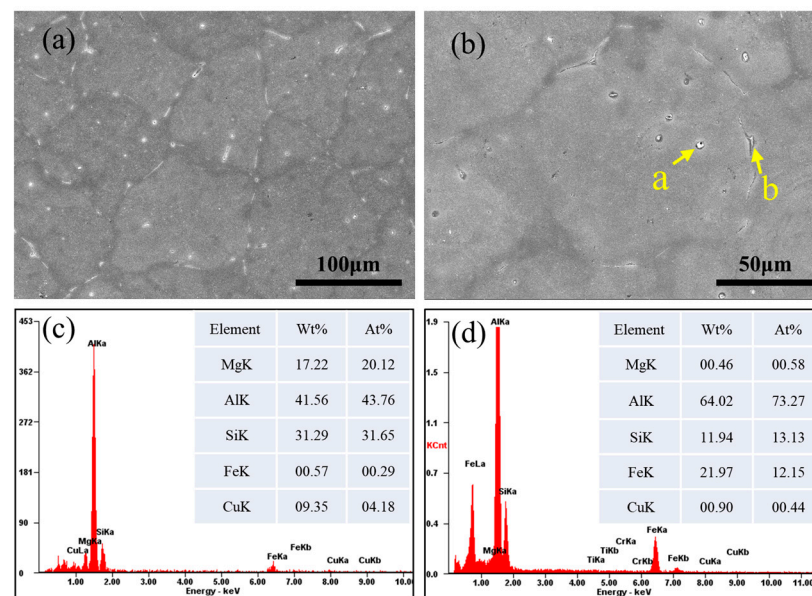
Figure 2 shows the effect of the homogenization process on the microstructure of the alloy. As can be seen in Figure 2a, the as-cast alloy exhibits severe segregation and non-equilibrium eutectic structure formed along grain boundaries. In addition, the hard-brittle second phase can lead to stress concentration, and decrease the thermal deformation ability of the alloy [16]. Therefore, the cast alloy needs to be homogenized to eliminate elemental segregation and avoid affecting the properties of the extruded alloys. As shown in Figure 2b, equiaxed recrystallized grains were formed in the homogenized alloy, and the grain boundaries were relatively straight, indicating a supersaturated state. It is clear that most of the eutectic and second phases dissolved into the matrix, which can reduce the deformation resistance and facilitate hot extrusion deformation [17–19].



**Figure 2.** Effect of homogenization on Al-0.5Mg-0.4Si-0.1Cu alloy: (a) as-cast, (b) homogenized.

In order to further study the effect of homogenization on the typical second phase in the as-cast alloy, the morphology and composition of the second phase were characterized

by SEM and Energy Dispersive Spectrometer (EDS) scanning. As shown in Figure 3, a large number of needle-like and spherical second phases (yellow arrows) were found in the alloy, distributed at grain boundaries and within the grain. Figure 3c shows the EDS scanning result of the spherical second phase (marked position at point a), which pointed out that the phase is a Cu-rich phase (Q phase). In addition, the EDS scanning results of the acicular phase are shown in Figure 3d, whose components mainly include Al, Fe, and Si. According to the morphological characteristics and atomic ratio of Fe and Si (0.9), it can be known that the acicular phase is mainly the  $\beta$ -AlFeSi phase. During the thermal deformation of the alloy, such as extrusion and rolling, the  $\beta$ -AlFeSi phase causes matrix splitting, which is very unfavorable to the plastic forming of the alloy.



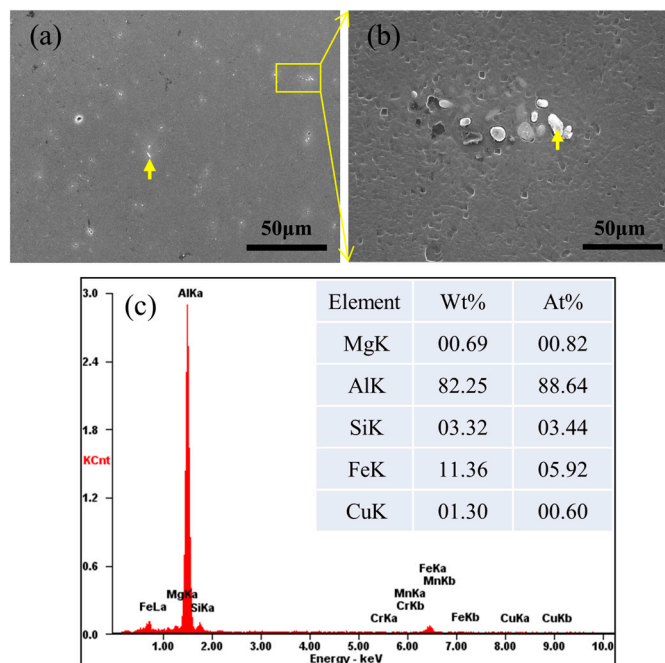
**Figure 3.** (a,b) Microstructure of as-cast alloy; (c) composition at point (a); (d) composition at point (b).

Figure 4 shows SEM images and EDS scanning of the homogenized alloy. It can be seen that the segregation in the as-cast alloy has been largely eliminated after homogenization. The second phase particles are significantly refined and uniformly distributed in the alloy matrix. As shown in Figure 4c, the content of aluminum in the second phase increases, while the content of elements such as Mg and Si decreases. The atomic ratio of Fe to Si is about 1.72, which indicates that the Fe-rich phase belongs to  $\alpha$ -AlFeSi. The above results indicate that the needle-like  $\beta$ -AlFeSi phase in the cast alloy has evolved into a granular  $\alpha$ -AlFeSi phase during homogenization. The transformation of the second phase will be more favorable for the subsequent hot working deformation. On the other hand, no Cu-rich phases were found in the homogenized alloy, indicating that most of the eutectic phase with a low melting point has been dissolved into the matrix during homogenization. Only a few of the  $\alpha$ -AlFeSi phases remain in the alloy, indicating that a high degree of homogenization has been achieved.

### 3.2. Microstructure of Extruded Alloys

In order to investigate the relationship between the extrusion ratio and the microstructure of extruded alloys, OM and EBSD tests were applied. The microstructure parallel and perpendicular to the extrusion direction (ED) is shown in Figure 5. It can be seen that the grains were obviously refined with the extrusion ratio increasing. When the extrusion ratio is 7 and 13, as shown in Figure 5a,c, the grains of extruded alloys are equiaxed and grain boundaries are smooth (blue arrows). Compared to the large grains (220 μm) of the alloy before extrusion, average grain sizes of extruded alloys ( $\lambda = 7, 13$ ) were reduced to 160 μm and 122 μm, respectively. As shown in Figure 5f, although the average grain size is only 85 μm when the extrusion ratio is 21, the microstructure uniformity is poor,

which adversely affects the mechanical properties of the alloy. It is noteworthy that grains were further refined ( $45\ \mu\text{m}$ ) when the extrusion ratio is 30, as shown in Figure 5h, and microstructure uniformity is also improved.



**Figure 4.** (a,b) Microstructure of the homogenized alloy; (c) composition of second phase.

Figure 6 shows the EBSD maps and misorientation angle distribution along the extrusion direction. It should be noted that white lines correspond to low-angle grain boundaries (LAGB) with orientation angles between  $2^\circ$  and  $15^\circ$ . Moreover, the thicker black lines represent high-angle grain boundaries (HAGB) with orientation angles greater than  $15^\circ$ . When the extrusion ratio is 7, as shown in Figure 6a, the grains are stretched along the extrusion direction. Meanwhile, the presence of a large amount of LAGB inside the grains indicates that dynamic recovery (DRV) occurred in the extruded alloy [20–22]. With continued deformation, discontinuous dynamic recrystallization (DDR) grains will nucleate and grow at the grain boundaries of the original grains [23]. As shown in Figure 6a, the recrystallization degree under the present condition is low, and only a few equiaxed grains with non-uniform sizes are formed. Similarly, when the extrusion ratio was 13, as shown in Figure 6c, there are still a large of fibrous structures existed inside the alloy, but the DRX degree has been improved and the number of recrystallization grains increased. Figure 6b,d shows statistical results of grain boundaries orientation of the alloys with the extrusion ratio of 7 and 13. It is clear that the vast majority of the orientation angles are obviously concentrated in the range of LAGB ( $2^\circ\sim 15^\circ$ ) and the proportions of HAGB are about 13.68% and 17.64%, respectively.

Generally, during the hot extrusion process, certain deformation amounts and deformation temperatures are needed for the aluminum alloy to achieve full dynamic recrystallization [24–27]. When the extrusion ratio reached 21, as shown in Figure 6e, the deformed structure almost disappeared and the number of equiaxed DRX grains was greatly increased, and the proportion of HAGB increased to 38.79% (Figure 6f). However, uneven microstructure and softening effect of recrystallization will lead to a decrease in mechanical properties. Continuing to increase the extrusion ratio to 30, as shown in Figure 6g, dynamic recrystallization of the alloy is more sufficient and the structure is more uniform. Moreover, the recrystallized grain size is significantly reduced, indicating that the extrusion ratio has a significant effect on grain refinement [28,29]. While, the proportion of LAGB and HAGB change little, with 39.81% for HAGB (Figure 6h).

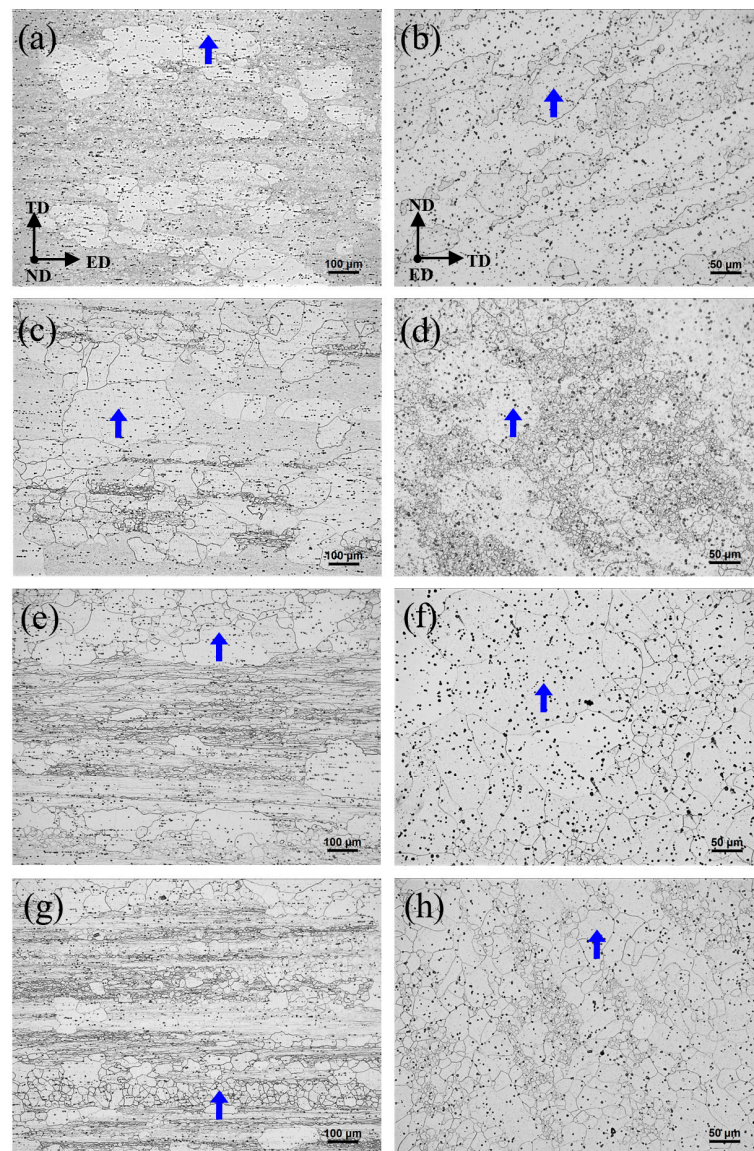


**Figure 5.** Microstructure of the extruded alloys: (a,b)  $\lambda = 7$ , (c,d)  $\lambda = 13$ , (e,f)  $\lambda = 21$ , (g,h)  $\lambda = 30$ .

Figure 7 shows the DRX distribution and statistical results of the extruded alloys, which intuitively show the effect of extrusion ratios on microstructure evolution by coloring deformed microstructure, substructure and recrystallized grains. It can be seen that when the extrusion ratio was 7, as shown in Figure 7a, most of the extruded alloy consisted of a deformed microstructure (red region). As can be seen from the bar graph on the right, the proportion of recrystallized grains (blue region) was only 33%. When the extrusion ratio was 13, as shown in Figure 7b, the proportion of recrystallized grains increased significantly to 59.4%. Continuing to increase the extrusion ratio to 21 and 30 (Figure 7c,d), the proportion of recrystallized grains reached more than 90%.

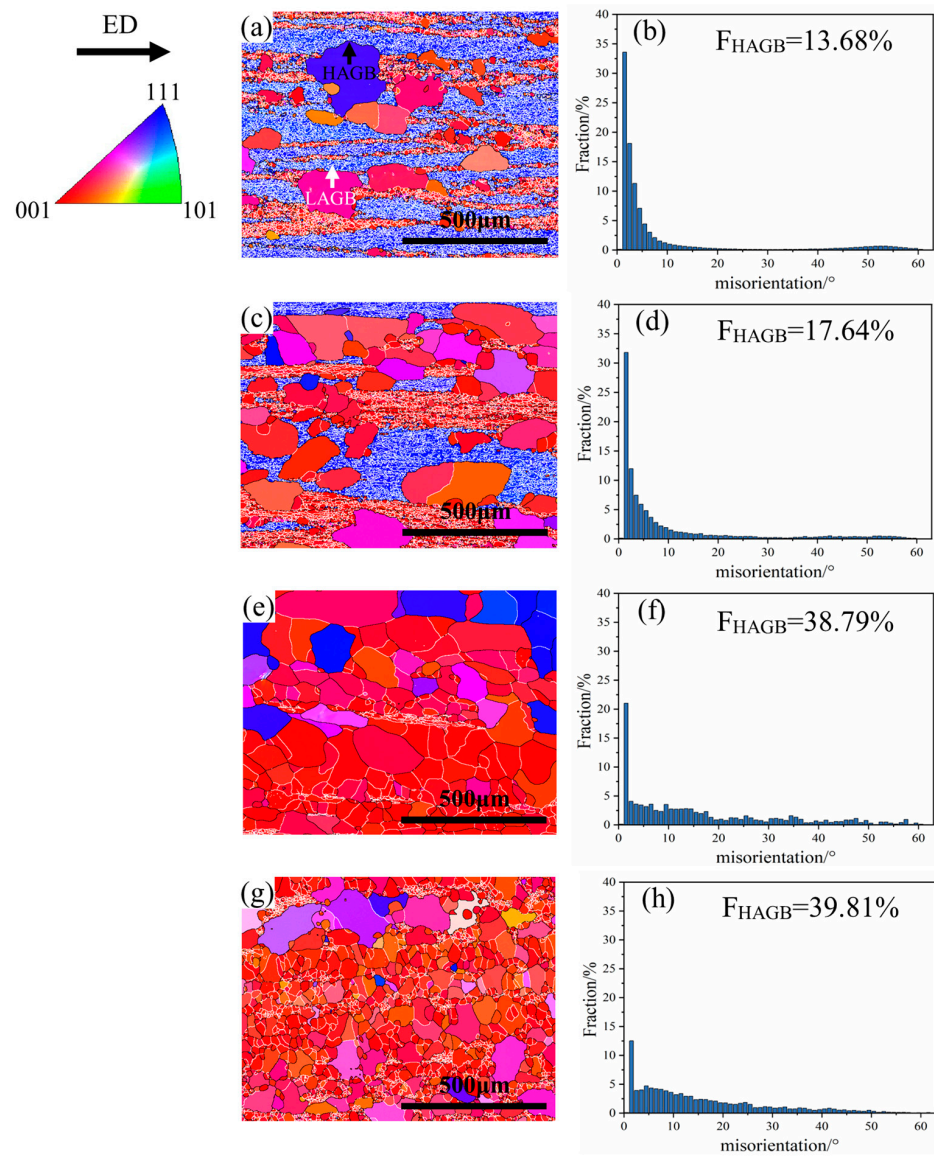


**Figure 6.** EBSD maps and misorientation angle distribution of specimens: (a,b)  $\lambda = 7$ , (c,d)  $\lambda = 13$ , (e,f)  $\lambda = 21$ , (g,h)  $\lambda = 30$ .

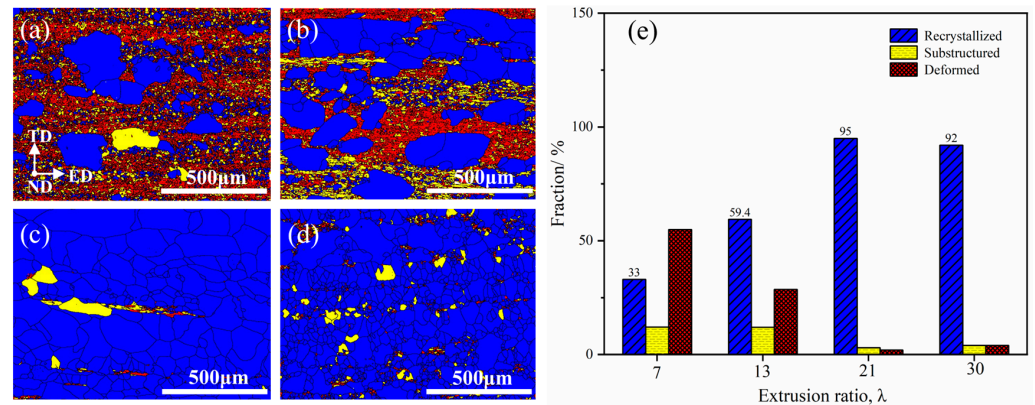


**Figure 7.** DRX distribution and statistical results of extruded alloys: (a)  $\lambda = 7$ , (b)  $\lambda = 13$ , (c)  $\lambda = 21$ , (d)  $\lambda = 30$ ; (e) Statistical plot of DRX content.

### 3.3. Texture Analysis

Figure 8 shows the inverse pole figures (IPF) of the extruded alloys. It can be seen that the textures are mainly concentrated in  $\langle 111 \rangle$  and  $\langle 001 \rangle$  orientations. It is known that when metals undergo plastic deformation, their crystal orientation will constantly transform from soft orientation (large orientation factor) to hard orientation (small orientation factor) [30]. Therefore, during the hot extrusion deformation process, for a face-centered cubic crystal, its orientation factor reaches the minimum value when the crystal orientation  $\langle 111 \rangle$  is parallel to the extrusion direction. Continue to increase the deformation process, the grains with other orientations gradually move to  $\langle 111 \rangle$  orientation and form a strong preferred orientation. When the extrusion is 7, as shown in Figure 8a, the texture strength (Concentration degree of grains in a certain orientation) in  $\langle 111 \rangle$  orientation is the largest, which is 14.97 (white number). With the extrusion ratio increasing to 13, as shown in Figure 8b, the recrystallization texture of  $\langle 001 \rangle$  orientation is enhanced with the increase of recrystallization degree which is 9.24. On the contrary, the texture strength of  $\langle 111 \rangle$  orientation decreases to 6.02. At this time, neither texture is fully developed. When the extrusion is 21, as shown in Figure 8c, texture strength of  $\langle 111 \rangle$  orientation is further weakened to only 2.71, while recrystallization texture strength reaches 16.68, indicating crystals produce stronger meritocratic orientation under greater plastic deformation. When the extrusion ratio increased to 30, as shown in Figure 8d, the texture of  $\langle 111 \rangle$  orientation almost disappeared. Similar results have been reported where the recrystallization degree of alloys increased with the extrusion ratio increasing, while the texture of  $\langle 111 \rangle$  orientation disappeared [31]. Meanwhile, the texture intensity of  $\langle 001 \rangle$  orientation was reduced to 9.78 due to the increase in grain boundaries caused by grain refinement. During the extrusion deformation process, fine grains are more prone to rotation, which promotes grain boundary migration and weakens the consistency of grain orientations. Moreover, a decrease in anisotropy improves the plasticity of extruded alloys [32].

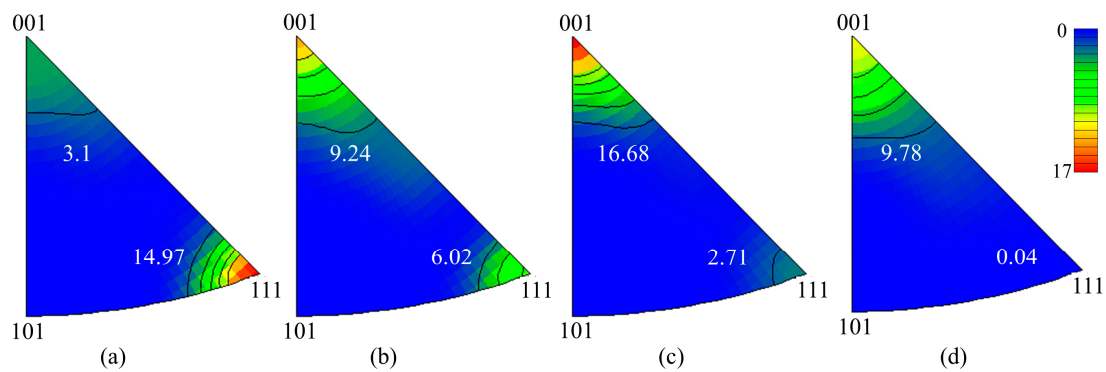


**Figure 8.** IPF of the extruded alloys: (a)  $\lambda = 7$ , (b)  $\lambda = 13$ , (c)  $\lambda = 21$ , (d)  $\lambda = 30$ .

### 3.4. Tensile Properties

The tensile properties of the extruded alloys are shown in Figure 9. In terms of the overall change trend, tensile properties gradually increased with the extrusion ratio increasing. Generally, the improvement of mechanical properties is mainly attributed to grain refinement, texture and the second phase [33]. If only the texture is considered, the low texture strength of the alloy at an extrusion ratio of 30 predicts a decrease in its tensile strength. However, the stress-strain curves show that the mechanical properties of the alloy with an extrusion ratio of 30 are better, indicating that the strengthening effect of texture is less than grain size and uniformity on the alloy with an extrusion ratio of 21. Among the various factors, the average grain size plays a crucial role in the mechanical properties of the alloy, and fine grains can lead to high strengthening effects [34]. When the extrusion ratio is 30, due to the decrease in the average grain size, the tensile strength and elongation of the alloy increased to 152 MPa and 32.4%, respectively. It is worth noting that the difference in mechanical properties of the alloy is small when the extrusion ratio is 13

and 30. The main reason is the difference in their reinforcement mechanisms. When the extrusion ratio is 13, the dynamic recrystallization degree is low and work-hardened plays a major role. A higher degree of dynamic recrystallisation occurred in the alloy with the extrusion ratio of 30, which can lead to some softening of the alloy, while, due to fine grain strengthening the strength can partly increase.

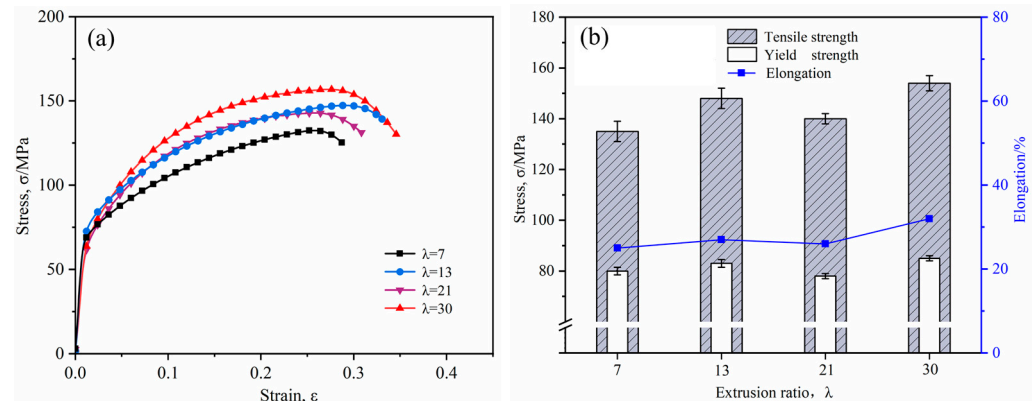


**Figure 9.** Effect of extrusion ratio on the tensile properties of the alloys: (a) Stress-strain curves; (b) Histogram of tensile properties.

Tensile test results showed that the elongation of the extruded alloys reaches more than 20%, indicating that the alloy has good plasticity which is consistent with the presence of a large number of dimples on the fracture surface of the extruded alloy (Figure 10). It can be seen that the fracture morphology of the alloy varies at different extrusion ratios.

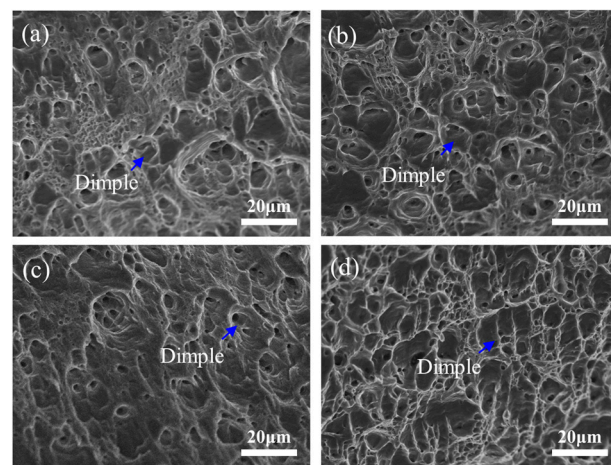


**Figure 10.** SEM images of tensile fracture of extruded alloys: (a)  $\lambda = 7$ , (b)  $\lambda = 13$ , (c)  $\lambda = 21$ , (d)  $\lambda = 30$ .

When the extrusion ratio was increased from 7 to 13, as shown in Figure 10a,b, the uniformity of dimples on the surface of the tensile fracture has been improved. However, when the extrusion ratio was increased to 21, as shown in Figure 10c, the dimples gradually became larger and shallower, possessing a corresponding lower elongation, which is consistent with the tensile test results. When the extrusion ratio was increased to 30, as shown in Figure 10d, the dimples increased significantly and are more uniform, showing excellent elongation [35].

### 3.5. Microstructure Evolution during Hot Extrusion

Generally, during the hot extrusion process, a great number of dislocations will proliferate in the alloy and its density will increase rapidly due to the intense plastic deformation. Meanwhile, sub-grains are important structural features formed by dislocation motion during the severe plastic deformation process and its dynamic evolution process is closely

related to dynamic recovery and dynamic recrystallization [36]. It is reported that when an alloy was deformed, high-density dislocations are gradually accumulated around the second phase and a distortion zone with a high orientation gradient will form near it, which can provide a driving force for DRX and similar phenomena appears in this work [37]. When the extrusion ratio is 7, as shown in Figure 11a, dislocation movement is pinned and inhibited by the second phase, resulting in dislocation accumulation. Figure 11d shows the high-resolution morphology of the second phase, followed by calibration of its diffraction spot (Figure 11g) the phases are nanoscale  $\text{Al}_8\text{Fe}_2\text{Si}$ . It can be seen in Figure 11b, a sub-grain prototype was found in the alloy of extrusion ratio is 13 with a significantly reduced dislocation density. The formation of sub-grains is due to dynamic recovery. As the deformation continues, more dislocations will move to grain boundaries or dislocation walls, resulting in dislocations balance out and recombination which will leave the same type of dislocations to reduce dislocation spacing (Figure 11h), and dislocation walls will gradually become clear and transform into sub-grain boundaries [38]. Figure 11e shows the high-resolution morphology of sub-grain boundaries and it can be seen that under the effect of deformation stress, many crystalline defects such as vacancies generated and it is favorable for dislocations to slip and climb, which will lead to the formation of LAGB. In addition, a black iron-rich phase was also found along the boundary (Figure 11b), indicating that the second phase can limit the movement of sub-grains. When the extrusion ratio is lower, sub-grains do not have enough driving force to get rid of the pinning effect of the second phase, which will delay the DRX process and prevent the rapid formation of recrystallized grains from sub-grains. It follows that the microstructure evolution of the alloy during thermal deformation is multivariate and complex. It has been reported that work hardening and dynamic softening jointly determine the strength and plasticity of aluminum alloys [39]. Due to the pinning effect of the second relative dislocation, the alloy has a high deformation resistance which compensates for the negative effect of dynamic softening on the strength.

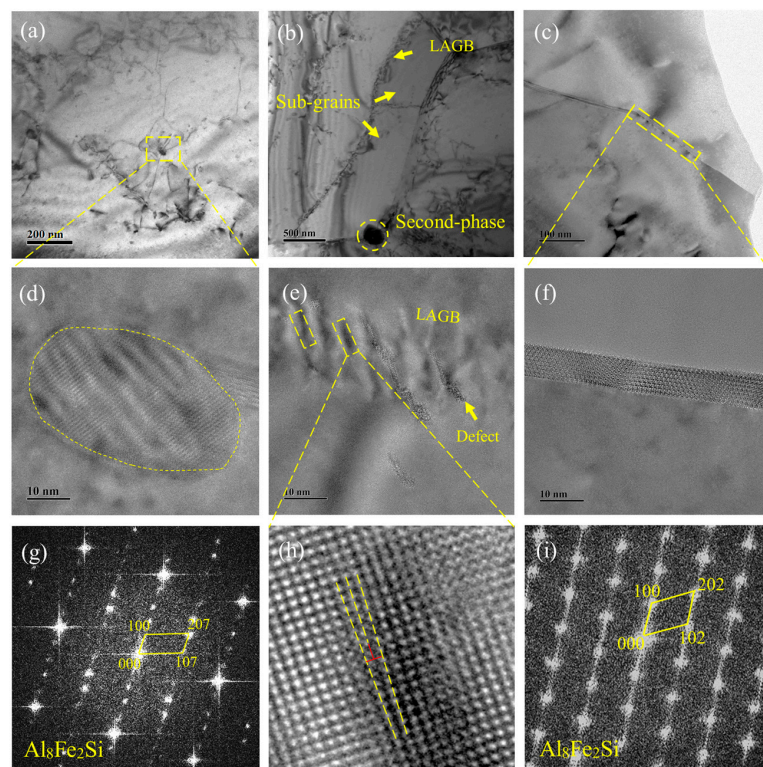


**Figure 11.** TEM images of the extruded alloy under different extrusion ratios: (a,d,g)  $\lambda = 7$ , (b,e,h)  $\lambda = 13$ , (c,f,i)  $\lambda = 30$ .

On the other hand, it has been reported that nanoparticles distributed along grain boundaries not only inhibit the DRX process but also hinder the migration process of HAGB after deformation [40]. Figure 11c shows the TEM image of the alloy with an extrusion ratio of 30, where the  $\text{Al}_8\text{Fe}_2\text{Si}$  phase is also found at the grain boundary (Figure 11f,i) and the dislocation density is greatly reduced due to the DRX process. It can be seen that an increased extrusion ratio can refine the grains, and the limitation of the migration of HAGB by second-phase particles also plays a role in avoiding grain coarsening. More importantly, refined grains provide a large amount of grain boundaries, which can effectively impede the slip of grain boundaries, resulting in more uniformly stressed during deformation and excellent fracture toughness [41].

#### 4. Conclusions

In this work, the effect of extrusion ratios on microstructure and mechanical properties of Al-0.5Mg-0.4Si-0.1Cu alloy was studied and the following results were obtained:

- (1) When the extrusion ratio was low, softening mechanism of the alloy was mainly DRV and the original grains were elongated along the ED direction. With the extrusion ratio increasing from 7 to 30, the proportion of dynamically recrystallized grains increased from 33% to 92%, the average grain size decreases from 160  $\mu\text{m}$  to 45  $\mu\text{m}$ .
- (2) The textures of the alloy are mainly concentrated in  $\langle 111 \rangle$  and  $\langle 001 \rangle$  orientations. With the increasing extrusion ratio, the texture of  $\langle 001 \rangle$  orientation gradually occupied the main position, texture intensity of  $\langle 111 \rangle$  orientation decreased after DRX fully developed. The presence of nano-sized  $\text{Al}_8\text{Fe}_2\text{Si}$  particles caused dislocation pile-up which provided a driving force for DRX and also limited the migration of HAGB.
- (3) When the extrusion ratio was increased from 7 to 30, the dimples on the tensile fracture surface increased and are more uniform, showing excellent elongation of 32.4%. Due to the fine-grain strengthening mechanism, the tensile strength of the alloy with an extrusion ratio of 30 reached 152 MPa.

**Author Contributions:** Conceptualization, X.X., J.D. (Jian Ding) and Y.L.; methodology, X.X. and J.D. (Jian Ding); validation, J.W.; formal analysis, C.N. and J.D. (Jian Ding); investigation, J.D. (Jiahang Dai); data curation, C.N., J.D. (Jiahang Dai) and Y.W.; writing—original draft preparation, C.N.; writing—review and editing, X.X. and J.D. (Jian Ding); visualization, X.X.; supervision, X.X., J.D. (Jian Ding) and Y.L.; project administration, X.X. All authors have read and agreed to the published version of the manuscript.

**Funding:** This research was funded by the National Key R&D Program of China (Grant No. 2018YFB2001800), Military-civilian integration project of Hebei Province, Key R&D Program of Hebei Province (No. 22351003D) and Natural Science Foundation of Hebei Province (No. E2019202161 and No. E2021202091).

**Data Availability Statement:** Data is unavailable due to privacy or ethical restrictions.

**Conflicts of Interest:** The authors declare no conflict of interest.

#### References

1. Li, J.; Ye, Z.; Fu, J.; Qi, W.; Tian, Y.; Liu, L.; Wang, X. Microstructure evolution, texture and laser surface HEACs of Al-Mg-Si alloy for light automobile parts. *Mater. Charact.* **2020**, *160*, 110093. [[CrossRef](#)]
2. Wang, X.F.; Guo, M.X.; Zhang, Y.; Xing, H.; Li, Y.; Luo, J.; Zhang, J.S.; Zhuang, L.Z. The dependence of microstructure, texture evolution and mechanical properties of Al-Mg-Si-Cu alloy sheet on final cold rolling deformation. *J. Alloys Compd.* **2016**, *657*, 906–916. [[CrossRef](#)]
3. Miller, W.S.; Zhuang, L.; Bottema, J.; Wittebrood, A.J.; Smet, P.D.; Haszler, A.; Vieregge, A. Recent development in aluminum alloys for the automotive industry. *Mater. Sci. Eng. A* **2000**, *280*, 37–49. [[CrossRef](#)]
4. Zhang, H.; Lin, G.; Peng, D.; Yang, L.; Lin, Q. Dynamic and static softening behaviors of aluminum alloys during multistage hot deformation. *J. Mater. Process. Technol.* **2004**, *148*, 245–249. [[CrossRef](#)]
5. Wang, B.; Liu, X.; Zhu, Y.; Ma, C.; Qiu, F.; Zhao, Q.; Jiang, Q. The effect of Mg/Si ratio on the microstructure and tensile properties of twin-roll casting Al-Mg-Si alloys. *Mater. Charact.* **2022**, *191*, 112146. [[CrossRef](#)]

6. Zhou, M.Z.; Wen, B.Y.; Ding, L.P. Effect of Mg/Si ratio on natural aging and precipitation strengthening of 6000 series aluminum alloys. *T. Mater. Heat. Treat.* **2015**, *36*, 68–72.
7. Tao, G.H.; Liu, C.H.; Chen, J.H.; Lai, Y.X.; Ma, P.P.; Liu, L.M. The influence of Mg/Si ratio on the negative natural aging effect in Al-Mg-Si-Cu alloys. *Mater. Sci. Eng. A* **2015**, *642*, 241–248. [[CrossRef](#)]
8. Zhang, T.P.; Xiong, J.; Wang, J.; Yang, Q.P.; Zhong, Y. Effect of rare earth on microstructure and extrusion properties of 6061 aluminum alloy. *Light Alloy Fabr. Technol.* **2010**, *38*, 33–35.
9. Chang, L.; Ding, Y.; Guo, B.; Ding, J.; Xia, X.; Tang, Y.; Li, C.; Sun, X.; Guo, J.; Song, K.; et al. Modification mechanism and tensile property of Al-9Si-0.4Mg-0.1Cu alloy. *Mater. Charact.* **2022**, *184*, 111693. [[CrossRef](#)]
10. Ding, W.; Zhao, X.; Chen, T.; Zhang, H.; Liu, X.; Cheng, Y.; Lei, D. Effect of rare earth Y and Al-Ti-B master alloy on the microstructure and mechanical properties of 6063 aluminum alloy. *J. Alloy Compd.* **2020**, *830*, 154685. [[CrossRef](#)]
11. Chang, L.; Zhao, Q.; Xia, X.; Ding, Y.; Guo, B.; Ding, J.; Tang, Y.; Zhang, Z.; Li, C.; Sun, X.; et al. Modification Mechanism and Uniaxial Fatigue Performances of A356.2 Alloy Treated by Al-Sr-La Composite Refinement-Modification Agent. *Acta Met. Sin.* **2022**, *35*, 901–914. [[CrossRef](#)]
12. Liu, C.; Zhang, J.B.; Yang, Y.K.; Tang, Y.; Zhang, Z.; Chen, X.G.; Liu, Y.C. Hot Deformation Behavior of ATI 718Plus Alloy with Different Microstructures. *Acta Metall. Sin.* **2022**, *35*, 1383–1396. [[CrossRef](#)]
13. Cao, G.H.; Yu, Z.H.; Zhang, D.T.; Zhu, S.A.; Xiang, S.Q. Effect of extrusion ratio on microstructure and mechanical properties of 6063 aluminum. *Light Alloy Fabr. Technol.* **2022**, *50*, 37–41.
14. Zhang, C.; Wang, C.; Zhang, Q.; Zhao, G.; Chen, L. Influence of extrusion parameters on microstructure, texture, and second-phase particles in an Al-Mg-Si alloy. *J. Mater. Process. Technol.* **2019**, *270*, 323–334. [[CrossRef](#)]
15. Yi, H.; Ding, J.; Ni, C.A.; Dai, J.H.; Tang, Y.; Chen, X.G.; Song, K.H.; Xia, X.C. Hot compression deformation behavior and processing maps of Al-0.5Mg-0.4Si-0.1Cu alloy. *J. Mater. Res. Technol.* **2022**, *19*, 4890–4904. [[CrossRef](#)]
16. Ding, W.J.; Jin, L.; Lin, D.L.; Zeng, X.Q.; Mao, D.L. Effect of Second Phase on the Mechanical Properties of Mg-Al-Zn Alloy by Equal Channel Angular Extrusion. *Mater. Sci. Forum* **2007**, *62*, 546–549.
17. Arnoldt, A.R.; Schiffl, A.; Höppel, H.W.; Österreicher, J.A. Influence of different homogenization heat treatments on the microstructure and hot flow stress of the aluminum alloy AA6082. *Mater. Charact.* **2022**, *191*, 112129. [[CrossRef](#)]
18. Guo, X.B.; Chang, L.; Dai, J.H.; Ding, Y.M.; Li, R.; Ding, J.; Li, C.; Tang, Y.; Xia, X.X.; Chen, X.G.; et al. Effect of Heat Treatment on the Microstructure and Mechanical Properties of Al-9Si-0.4Mg-0.1Cu Alloy. *Adv. Eng. Mater.* **2022**, *24*, 2200569. [[CrossRef](#)]
19. Qian, X.; Parson, N.; Chen, X.-G. Effect of Homogenization Treatment and Microalloying with Mn on the Microstructure and Hot Workability of AA6060 Aluminum Alloys. *J. Mater. Eng. Perform.* **2019**, *28*, 4531–4542. [[CrossRef](#)]
20. Qu, J.; Xie, X.; Bi, Z.; Du, J.; Zhang, M. Hot deformation characteristics and dynamic recrystallization mechanism of GH4730 Ni-based superalloy. *J. Alloy Compd.* **2019**, *785*, 918–924. [[CrossRef](#)]
21. Wen, D.-X.; Lin, Y.; Li, X.-H.; Singh, S.K. Hot deformation characteristics and dislocation substructure evolution of a nickel-base alloy considering effects of  $\delta$  phase. *J. Alloy Compd.* **2018**, *764*, 1008–1020. [[CrossRef](#)]
22. Lu, J.; Song, Y.; Hua, L.; Liu, J.; Shen, Y. Influence of thermal deformation conditions on the microstructure and mechanical properties of boron steel. *Mater. Sci. Eng. A* **2017**, *701*, 328–337. [[CrossRef](#)]
23. Zhong, X.T.; Wang, L.; Liu, F. Study on Formation Mechanism of Necklace Structure in Discontinuous Dynamic Recrystallization of Incoloy 028. *Acta Metall. Sin.* **2018**, *54*, 969–980.
24. Chen, W.; Guan, Y.P.; Wang, Z.H. Investigation on Dynamic Recrystallization Critical Strain of Al-Mg-Si-Ti Alloy Under Certain Conditions. *Mater. Rev.* **2016**, *30*, 164–168.
25. Zhang, H.; Li, L.X.; Yuan, D.; Peng, D.S. Hot deformation behavior of the new Al-Mg-Si-Cu aluminum alloy during compression at elevated temperatures. *Mater. Charact.* **2007**, *58*, 168–173. [[CrossRef](#)]
26. Lee, J.W.; Son, K.T.; Jung, T.K.; Yoon, Y.O.; Kim, S.K.; Choi, H.J.; Hyun, S.K. Continuous dynamic recrystallization behavior and kinetics of Al-Mg-Si alloy modified with CaO-added Mg. *Mater. Sci. Eng. A* **2016**, *673*, 648–659. [[CrossRef](#)]
27. Si, J.Y.; Han, P.B.; Chang, X.; Zhang, J. Recrystallization of Ti-46.5Al-2.5V-1.0Cr-0.3Ni alloy during hot forming. *J. Iron Steel Res. Int.* **2009**, *21*, 46–50.
28. Zhao, D.; Qin, J.; Lü, S.; Li, J.; Guo, W.; Wu, S.; Zhang, Y. Mechanisms of extrusion-ratio dependent ultrafine-grain fabrication in AZ31 magnesium alloy by continuous squeeze casting-extrusion. *J. Mater. Process. Technol.* **2022**, *310*, 117755. [[CrossRef](#)]
29. Zhao, Y.; Xu, C.; Taiki, N.; Shigeharu, K. Effect of extrusion ratio and temperature on microstructures and tensile properties of extruded Mg-Gd-Y-Mn-Sc alloy. *Mater. Sci. Eng. A* **2021**, *800*, 140330.
30. Hua, Q.; Zhang, Z.; Zhang, W.; Zhou, L. Influence of extrusion ratios on microstructure, texture and mechanical property of aluminum alloy 5154. *Forg. Stamping Technol.* **2018**, *43*, 154–159.
31. Kaneko, S.; Murakami, K.; Sakai, T. Effect of the extrusion conditions on microstructure evolution of the extruded Al-Mg-Si-Cu alloy rods. *Mater. Sci. Eng. A* **2009**, *500*, 8–15. [[CrossRef](#)]
32. Chen, Z.H.; Xu, F.Y.; Fu, D.F.; Xia, W.J. Dynamic recrystallization of magnesium alloy. *Chem. Ind. Eng. Prog.* **2006**, *25*, 140–146.
33. Wang, H.; Rong, J.; Liu, G.; Zha, M.; Wang, C.; Luo, D.; Jiang, Q. Effects of Zn on the microstructure and tensile properties of as-extruded Mg-8Al-2Sn alloy. *Mater. Sci. Eng. A* **2017**, *698*, 249–255. [[CrossRef](#)]
34. Khelfa, T.; Rekik, M.A.; Muñoz-Bolaños, J.A.; Cabrera-Marrero, J.M.; Khitouni, M. Microstructure and strengthening mechanisms in an Al-Mg-Si alloy processed by equal channel angular pressing (ECAP). *Int. J. Adv. Manuf. Technol.* **2017**, *95*, 1165–1177.

35. Li, Z.; Chen, L.; Tang, J.; Zhao, G.; Zhang, C.; Chu, X. Microstructure evolution, plastic anisotropy, and intergranular corrosion of Al-Mg-Si sheet processed through a combination of hot extrusion and cold rolling. *Mater. Charact.* **2020**, *164*, 110299. [[CrossRef](#)]
36. Liu, S.; Pan, Q.; Li, M.; Wang, X.; He, X.; Li, X.; Peng, Z.; Lai, J. Microstructure evolution and physical-based diffusion constitutive analysis of Al-Mg-Si alloy during hot deformation. *Mater. Des.* **2019**, *184*, 108181. [[CrossRef](#)]
37. Humphreys, F.J. The nucleation of recrystallization at second phase particles in deformed aluminum. *Acta Metall.* **1977**, *25*, 323–1344. [[CrossRef](#)]
38. Güzel, A.; Jäger, A.; Parvizian, F.; Lambers, H.-G.; Tekkaya, A.; Svendsen, B.; Maier, H. A new method for determining dynamic grain structure evolution during hot aluminum extrusion. *J. Mater. Process. Technol.* **2012**, *212*, 323–330. [[CrossRef](#)]
39. Dai, R.J.; Deng, K.K.; Wang, C.J.; Nie, K.B.; Zhang, G.W.; Liang, W. Effects of precipitates and solute atoms on the work hardening and softening behavior of Zn-rich aluminum alloy. *Mater. Sci. Eng. A* **2022**, *848*, 143388. [[CrossRef](#)]
40. Qian, W.; Zhao, Y.; Kai, X.; Gao, X.; Jin, L.; Huang, L. Evolution of microstructure and mechanical properties influenced by nanosized precipitates during rolling deformation. *J. Alloys Compd.* **2020**, *858*, 157687. [[CrossRef](#)]
41. Du, Y.M.; Li, S.L.; Ai, X.G.; Xiao, Q.H. Research of strengthened iron and steel with second phase particle. *J. Iron Steel Res. Int.* **2020**, *32*, 683–689.

**Disclaimer/Publisher’s Note:** The statements, opinions and data contained in all publications are solely those of the individual author(s) and contributor(s) and not of MDPI and/or the editor(s). MDPI and/or the editor(s) disclaim responsibility for any injury to people or property resulting from any ideas, methods, instructions or products referred to in the content.